Structural, electrical and magnetic properties of the pyrochlorate $Er_{2-x}Sr_xRu_2O_7$ ($0 \le x \le 0.10$) system

A. Quiroz[a], E. Chavira[c], V. Garcia-Vazquez[b], G. González[c], and M. Abatal[a,*]

[a]*Facultad de Ingeniería Universidad Autónoma del Carmen,*
Av. Central S/N Esq. con Fracc. Mundo Maya, Ciudad del Carmen, Campeche, 24115 México
[b]*Instituto de Física Luis Rivera Terrazas, Benemérita Universidad Autónoma de Puebla,*
Apartado Postal J-48, Puebla, Pue., 72570, México.
[c]*Instituto de Investigaciones en Materiales, Universidad Nacional Autónoma de México,*
Apartado Postal 70-360 Ciudad de México, 04510 México.

In this research, we report a detailed study of the structural, electrical and magnetic properties of the ruthenium pyrochlore with the composition $(Er_{2-x}Sr_x)Ru_2O_7$ ($0 \le x \le 0.10$) prepared by solid-state reaction in air at ambient pressure. The synthesized products were characterized using powder X-ray diffraction. The structure of the samples was refined with the Rietveld method, showing that the lattice parameters are more sensitive to the Strontium and Erbium sites. Scanning electron microscopy shows that the crystal size varies between 0.27 and 0.62 μm. In all polycrystalline samples, the electrical resistance decreases with increasing temperature, indicating that the samples are nonmetallic. The slope of the temperature-dependent resistance profiles systematically decreases with increasing x, proving that the carrier concentration increases with increasing the Sr content. Zero-field-cooled and field cooled magnetization measurements show an irreversible behavior where the split is systematically enhanced by increasing x.

Keywords: Solid state chemistry; X-ray diffraction and scattering; spin glasses; other random magnets.

PACS: 82.33.Pt; 61.05.C-; 75.50.Lk

1. Introduction

Pyrochlore oxides have attracted considerable attention in many areas of Material Science during the last few decades, due to their chemical and structural flexibility as well as their wide range of properties, such as superconductivity [1,2], semi-conductivity [3], ionic conductivity [4,5], ferromagnetism [6] and luminescence [7,8]. Oxide ion-conducting pyrochlores find applications in solid oxide fuel cells as electrolytes [9,10] and gas sensors. During the last decade, there has been substantial interest in the use of pyrochlore oxides for nuclear waste disposal due to their high radiation resistance [11]. The structure and electronic properties of pyrochlore oxides depend on the disordering of cations and anions. The stability of the pyrochlore structure is generally decided by the ratio of ionic radii of cations at A and B sites [12]. These systems tend to get much more complicated when both the A and B sites are occupied by magnetic ions. These compounds show very interesting magnetic features, caused by the coupled magnetic interactions between the $4f$ electrons of rare earth, those between the d electrons of transition metals, and those between the d and f electrons [13]. For $Nd_2Ru_2O_7$, $Sm_2Ru_2O_7$, and $Eu_2Ru_2O_7$ compounds, there is evidence that has been reported for a spin-glass state below this temperature, as well as the coexistence of a weak ferromagnetic state with the spin glass state below 20 K [14]. In previous research [14-16], these compounds exhibit magnetic transitions for A = Pr, Nd, Sm, Eu and Y at 165, 150, 135, 120, and 145 K, respectively, suggesting that there are contributions to the magnetism from both the

trivalent rare earth and Ru^{4+}. In the rare-earth ruthenates ($A_2B_2O_7$) the small magnetic moment ($\approx 1 - 2\ \mu$B) associated with the Ru^{4+} ion ($S = 1$) has been proved to happen at a relatively high temperature between ≈ 70 and 160 K, depending on the ionic size of the rare-earth ion [17-18]. For example, solid solutions of $Bi_{2-x}Ln_xRu_2O_7$ (Ln = Pr - Lu) ($0 \le x \le 2$) system have been investigated previously for some lanthanides [19-21]. The unsubstituted $Bi_2Ru_2O_7$ compound is metallic and $Bi_{2-x}Ln_xRu_2O_7$ ($0 \le x \le 2$) solid solutions have been shown to cross a metal-semiconductor transition on increasing the rare-earth content x [21]. Thus, the modification and control of their electrical properties, ranging from a good metal to an insulator material, is essential for the development of functional applications. Therefore, considering the importance and potential applications of pyrochlores-type compounds, this work was focused on the study of the structural, electrical and magnetic properties of the $(Er_{2-x}Sr_x)Ru_2O_7$ system (ESRO), for $x = 0.0$, 0.02, 0.05, 0.07, and 0.10. With the incorporation of Sr^{2+} ions (atomic radii of 1.18 Å) stoichiometry and if, the coordination angle 130°C [22] is modified or this will have structural changes, that will be reflected in the electrical and magnetic properties of the system.

2. Experimental methods

Polycrystalline samples of the ESRO system were synthesized by solid-state reaction at ambient pressure in air. The starting materials were RuO_2 (Cerac, 99.9%), Er_2O_3 (Sigma-Aldrich, 99.9%) and $SrCO_3$ (Cerac, 99.9%). Structure and

purity of the starting materials were determined by XDR. Prior to weighing, $SrCO_3$ was preheated during 10-20 minutes at 120°C in order to dehydrate it. The stoichiometric mixture of the starting materials was done in air during 30 minutes, grinded with an agate mortar, resulting in homogenous slurry. The resultant ESRO mixture was compressed into pellets (13 mm diameter, $1.0 - 1.5 \pm 0.05$ mm thickness) by applying a pressure of 3 tons/cm^2 during 5 minutes under vacuum. The resulting compacted specimens were then sintered in air at 1200°C during 4 days and then cooled down to room temperature following the natural cooling of furnace to 6 h. Samples were characterized by X-ray powder diffraction (XRD) using an APD 2000 diffractometer with Cu Kα radiation ($\lambda = 1.5406$ Å) and a graphite monocromator. Diffraction patterns were collected at room temperature in air, over the 2θ range 10° - 90° with a step size of 0.025° and a time per step of 15 seconds. Rietveld refinement [23] was carried out using the FullPROF program [24]. Changes in morphology and grain size were induced in the samples by performing different heat treatments during all the process of the samples preparation and examined by scanning electron microscopy (SEM) on a Hitachi S-3400N-II System. The 15.00 K.X micrographs were taken with a voltage of 15 kV, a current intensity of 1000 pA and WD = 4.5 mm. Energy Dispersive X-Ray (EDX) was performed on the same SEM system, which is equipped with an EDAX 9900 device. Low temperature DC resistance measurements were performed using the standard four-probe method from room temperature down to 10 K. Magnetic properties were examined using a Quantum Design PPMS DynaCool-9 System with a vibrating sample magnetometer (VSM) option. Magnetic moment (M) versus temperature (T) measurements were performed at 360 to 2 K using fields up to ± 400 Oe.

3. Results and discussions

Figure 1 shows the XRD patterns of the sintered $Er_{2-x}Sr_xRu_2O_7$ ($0 \leq x \leq 0.10$) compounds. All samples crystallize in the cubic unit cell with $Fd\bar{3}m$ (# 227) space group and form a continuous solid solution. For the ESRO samples, it detected two phases that are identified as

$Er_2Ru_2O_7$ and Er_2O_3 compounds. The solid line corresponds to a cubic phase with $Fd\bar{3}m$ (# 227) space group and it is identified as $Er_2Ru_2O_7$ compound with PDF (72-7620). The phase marked with an asterisk (*) corresponds to the

Er_2O_3 compound, PDF (8-0050). The presence of this very small amount of Er_2O_3 compound was detected in the ESRO system then indicated that occur an overload of the reagent in all the system. This is presumably a consequence of loss of volatile ruthenium oxide [13]. The Rietveld analysis also indicates that there is no intermix between the Er^{3+} and the Ru^{4+} ions [13]. The individual bond lengths, x values and angle for the ESRO system are listed in Table I. These structural features are consistent with previous reports on rare-earth ruthenate pyrochlores [25]. The initial parameters of the pyrochlore phase $Er_2Ru_2O_7$ and the second phase Er_2O_3 reagent were taken from the results reported in [25-26]. The cubic lattice parameter a increases monotonously with strontium content x, in agreement with previous data (see below). The structural parameters with $Fd\bar{3}m$ space group were refined using a structural model, Er, 16c (0, 0, 0); Sr, 16c (0, 0, 0); Ru, 16d, (1/2, 1/2, 1/2); O(1), 48f, (x, 1/8, 1/8), $x = 0.4286$; O(2), 8a, (1/8, 1/8, 1/8). It is worth to mention that samples with $x = 0.02 - 0.10$ have not been previously reported in the literature. They show very weak reflections of a secondary phase, identified as Er_2O_3 compound PDF (8-0050). The other lattice parameters of $(Er_{2-x}Sr_x)Ru_2O_7$ system, $x = 0.0, 0.02, 0.05, 0.07,$ and 0.10, also vary with the inclusion of the Sr-ion content and Ru-ion coordination. They are consistent with the small difference between the
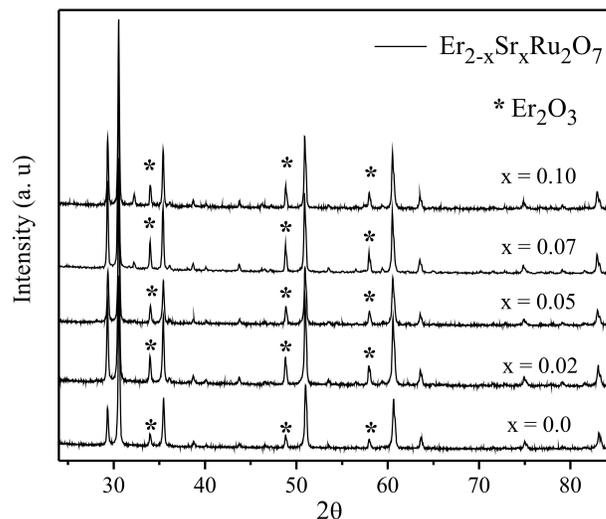

FIGURE 1. XDR Patterns evolution of $(Er_{2-x}Sr_x)Ru_2O_7$ system, with $x = 0.0, 0.02, 0.05, 0.07,$ and 0.10.

TABLE I. Summary of Rietveld refinements results in the $(Er_{2-x}Sr_x)Ru_2O_7$ $x = 0.0 - 0.10$ system; all distances in (Å) and angle (°).

x	a (Å)	Ru-O(1)	Er-O(2)	Er-O(1)	Ru-O(1)-Ru
0	10.124(8)	1.930(3)	2.192(1)	2.544(3)	136.01(2)
0.02	10.131(4)	1.931(5)	2.193(5)	2.545(9)	136.01(2)
0.05	10.141(8)	1.933(5)	2.195(7)	2.548(5)	136.01(2)
0.07	10.141(9)	1.933(5)	2.195(7)	2.548(5)	136.01(2)
0.10	10.143(1)	1.933(8)	2.196(0)	2.548(8)	136.01(2)
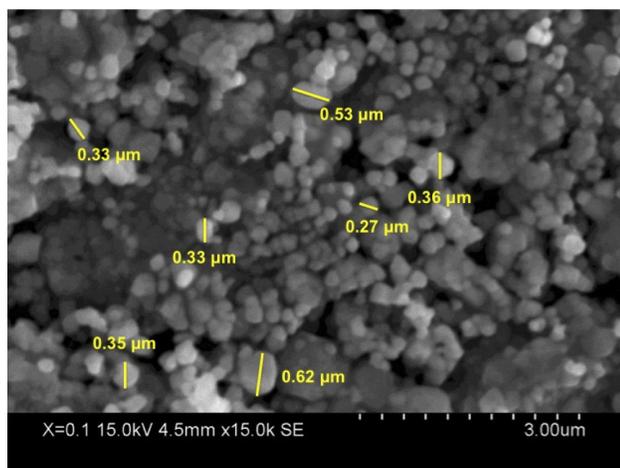
FIGURE 2. SEM of the $Er_{1.90}Sr_{0.10}Ru_2O_{6.95}$ sample.

FIGURE 3. The normalized electrical resistance as a function of temperature of $(Er_{2-x}Sr_x)Ru_2O_7$ system, with $x = 0.0, 0.02, 0.05, 0.07,$ and 0.10.

ionic radii of Er^{3+} at the Sr^{2+} ($Er^{3+} = 0.89$ Å and $Sr^{2+} = 1.18$ Å) [27]. We conclude that the Er^{3+} ions are substituted, partially (randomly, and intertitially) by Sr^{2+} ions with the observed in the structural parameters of each of the compounds.

Figure 2 shows the SEM image of the sample with $x = 0.10$. The image shows the effect of heat treatments and processing route on the grain morphology of the sample. Considerable variations in sizes, very few phases and shapes of polycrystals can be observed from the micrograph. The grain size varies between 0.27 μm to 0.62 μm. The micrographs were taken on the surface of the respective pellets of the ESRO samples with a magnification of 15.00 K.X. Also, in some regions a semi-fusion can be observed and may be attributed to the ruthenium content. We performed an EDX analysis on all samples to verify the chemical composition. The results are present in Table II. The error range of the analysis is between 1 and 6wt% [28]; therefore it can said that the experimental and theoretical atomic percentages of the elements resemble each other.

The electrical resistance as a function of temperature is presented in Fig. 3. All samples show a Mott insulating behavior. At a fixed, arbitrary temperature, the normalized resistance decreases with x, but seems saturated near $x = 0.10$, suggesting the solubility limit of the Sr^{2+} ion a substitution [29]. At a fixed temperature, the slope of the temperature-dependent resistance profiles systematically decreases with increasing x, indicating that the carrier concentration in-
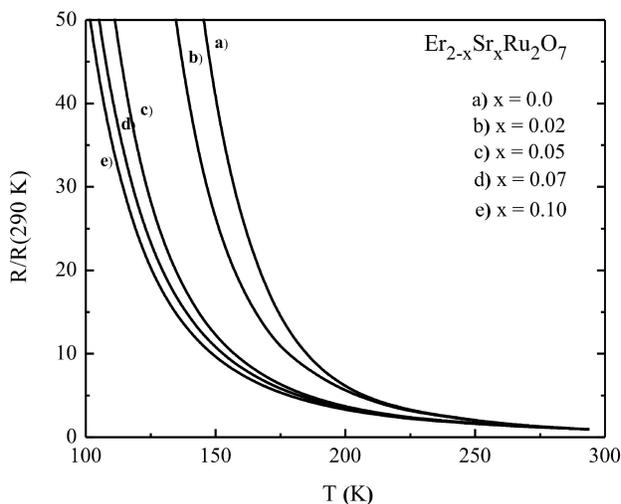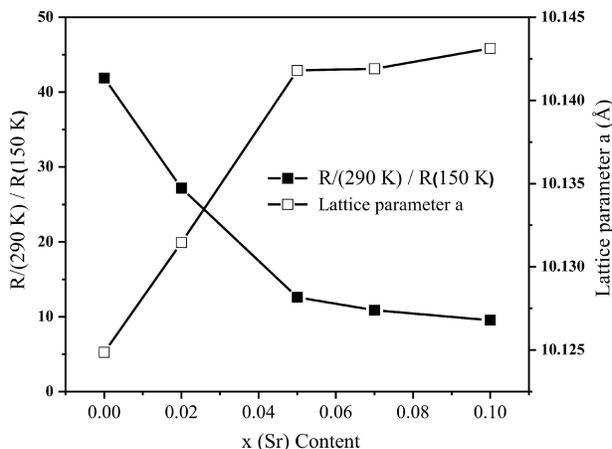

FIGURE 4. Resistance normalized variation and lattice parameter a of $(Er_{2-x}Sr_x)Ru_2O_7$ $x = 0.0 - 0.10$ system.

creases with increasing the Sr^{2+} ion content. These results show that the substituted Sr^{2+} ions act as a donor to supply electrons to the system. No metal transition was observed, however we attribute the spin-glass behavior to the substitution of Sr^{2+} at the Er^{3+} sites ($Sr^{2+} = 1.18$ Å and $Er^{3+} = 0.89$ Å) [30], changing the local electronic structure of the

TABLE II. EDX analysis of the $(Er_{2-x}Sr_x)Ru_2O_7$ $x = 0.0 - 0.10$ system.

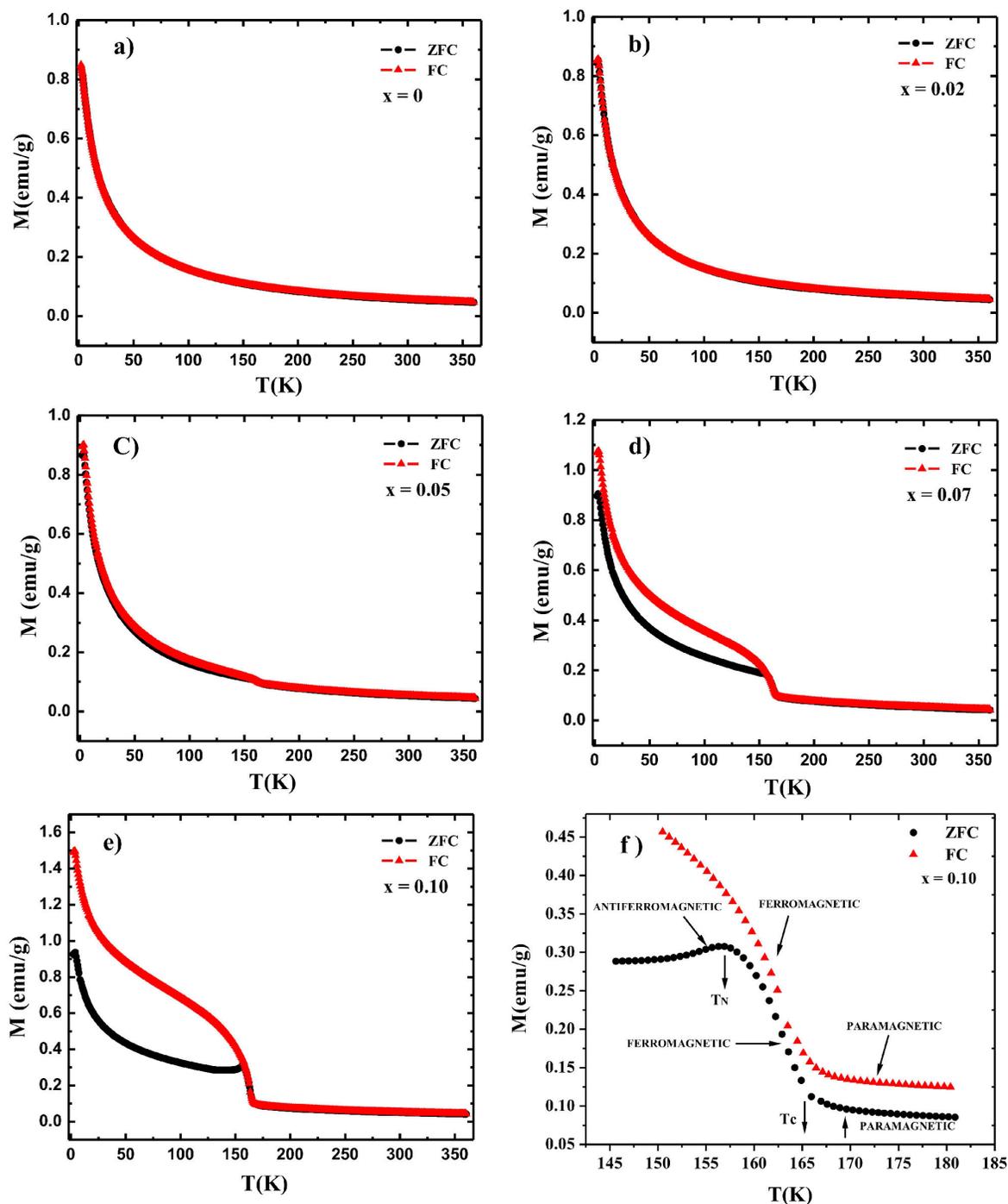|	ELEMENTS			
Samples	Er	Sr	Ru	O
$x = 0.0$	25.01 ($\pm$ 0.21)	0.0	18.97 ($\pm$0.32)	56.01 ($\pm$ 0.41)
$x = 0.02$	24.73 ($\pm$ 0.64)	1.04 ($\pm$0.18)	18.22 ($\pm$ 0.53)	56.02 ($\pm$ 0.67)
$x = 0.05$	22.56 ($\pm$ 0.48)	2.71 ($\pm$ 0.42)	17.45 ($\pm$ 0.37)	57.28 ($\pm$ 0.45)
$x = 0.07$	24.22 ($\pm$ 0.62)	2.41 ($\pm$ 0.43)	15.03 ($\pm$ 0.94)	58.34 ($\pm$ 0.41)
$x = 0.10$	21.43 ($\pm$ 0.39)	3.89 ($\pm$0.27)	17.60 ($\pm$ 0.30)	57.07 ($\pm$ 0.71)

FIGURE 5. Temperature dependence of moment magnetic (emu/g) for $(Er_{2-x}Sr_x)Ru_2O_7$ with $x = 0.0$, 0.02, 0.05, 0.07, and 0.10. The applied field for all the samples was 400 Oe.

Ru - O(1), Er - O(2) and Er - O(1) bonds lengths. Additionally is compensated with the oxygen content in Ru ion.

Figure 4 demonstrates the correlation between the cubic lattice parameter a and the residual resistance radio (RRR), defined here by the ratio of the resistance at 290 K and the resistance at 150 K. The parameter a increases monotonously with strontium content x, while the residual resistance radio (RRR) decreases exponentially with Sr^{2+} ions incoorporations. These effects occur in the lattice parameters and are related to the bond lengths Ru-O(1), Er-O(2) and Er-O(1). The changes in the distances Ru-O(1), Er-O(2) and Er-O(1) modify the electrical properties of our system, like can saw in the graphic.

Figure 5 demonstrate the temperature dependence of magnetization for $(Er_{2-x}Sr_x)Ru_2O_7$ ($0 \leq x \leq 0.10$) system measured at 400 Oe. Then the temperature dependence

of magnetic moments for the $Er_2Ru_2O_7$, and $Er_{1.98}Sr_{0.02}Ru_2O_{6.99}$ compounds were exhibited in the Fig. 5(a)-(b).

In these compounds, both the magnetic moments of the Er^{3+} and Ru^{4+} ions are in a magnetically ordered state. The present $Er_2Ru_2O_7$ compound don't affect the measurements. No significant difference between the ZFC and FC magnetic moments was observed in the whole temperature range. The origin for these magnetic moments between 2 and 360 K is that the paramagnetic moment for the Er^{3+} ions are induced by the Ru^{4+} ions when has a magnetic ordering. Moreover, the interaction between the Ru^{4+} and Er^{3+} ions may explain the long-range magnetic ordering of Er^{3+} ions at relatively higher temperature [13].

Figure 5(c) confirms the temperature dependence of the magnetic moment for $Er_{1.95}Sr_{0.05}Ru_2O_{6.975}$ compound. A magnetic transition at Tc≈165 K (Curie Temperature) is observed, below this transition temperature, there is slight divergence between the ZFC and FC magnetic moments. This inflection point is associated with a paramagnetic ordering below 165 K and above 165 K changes to a ferromagnetic ordering. This argument is justified by the substitution of Sr^{2+} ions for Er^{3+} ions, which modifies the network parameters and consequently modifies their magnetic properties by applying intense magnetic fields to lower temperatures.

Figure 5(e)-(d) illustrate the temperature dependence of magnetic moments for the $Er_{1.93}Sr_{0.07}Ru_2O_6.965$ and $Er_{1.90}Sr_{0.10}Ru_2O_{6.95}$ compounds measured at 400 Oe. Again a magnetic transition is observed at 165 K, like in Fig. 5(c) below this transition temperature, a remarkable divergence between the ZFC and FC magnetic moments is found. This inflection point is associated with a paramagnetic ordering below 165 K and above 165 K changes to a ferromagnetic ordering. However at a temperature of 157 K a new inflection point is presented which is related to an antiferromagnetic arrangement and is associated with TN (Néel Temperature). This magnetic behavior below 157 K indicates the onset of magnetic ordering between Ru^{4+} ions at short distances increasing for incorporation of Sr^{2+} ions. These arguments are again justified by the substitution partially (randomly, and intertitially) and increase of Sr^{2+} ions by Er^{3+} ions, which modifies the lattice, grain and shape size parameters (observed by SEM) and consequently modifies their magnetic moments to lower temperatures.

In Fig. 5 (f) we observed the behavior of the $Er_{1.90}Sr_{0.10}Ru_2O_{6.95}$ compound in the temperature range of 142 to 180 K between the ZFC and FC magnetic moments. This graph presents at FC an inflection point associated to paramagnetic ordering below 165 K and above 165 K changes to a ferromagnetic ordering, while for the same $Er_{1.90}Sr_{0.10}Ru_2O_{6.95}$ compound (Fig. 5(e)) but with ZFC presents a different behavior, this displays an antiferromagnetic ordering. It is well know that the magnetic transition in 157 K corresponds to the antiferromagnetic ordering of ruthenium moments associated to TN (Néel Temperature).

The high transition temperatures and the very large differences between the ZFC and FC magnetic moment indicate the existence of a very strong interaction between Ru^{4+} ions for incorporation of Sr^{2+} ions and the accommodation of the packing structural lattices.

Figure 5(f) we can observed the behavior of the $Er_{1.90}Sr_{0.10}Ru_2O_{6.95}$ composition in the temperature range of 142 to 180 K and the very large divergence between the ZFC and FC magnetic moment indicate the existence of a strong interaction between ruthenium ions at short distances increasing for incorporation of Sr^{2+} ions. This graph presents at FC an inflection point associated to paramagnetic ordering below 165 K and above 165 K changes to a ferromagnetic ordering, while for the same $Er_{1.90}Sr_{0.10}Ru_2O_{6.95}$ composition but with ZFC presents a different behavior, this displays an antiferromagnetic ordering. It is well know that the magnetic transition in 157 K corresponds to the antiferromagnetic ordering of ruthenium moments associated to TN (Néel Temperature). A mixture of phenomena, the magnetic behavior with the packing of the lattice in the final structure measured.

4. Conclusion

In this work, we obtained polycrystalline samples of ESRO system by solid-state reaction method in air at atmospheric pressure, in which a solubility up to $x = 0.10$ was observed. SEM micrographs exhibit an almost-spherical grain size distribution from 0.27 and 0.62 μm. The changes in the distances Ru-O(1), Er-O(2), and Er-O(1) modify the electrical properties of our system. The magnetic behavior of the ESRO system of each of the compounds was measured between ZFC and FC detecting the magnetic moments. The x value for $x = 0.0$ and $x = 0.02$ present a paramagnetic order and don't show any magnetic transition. However, when $x = 0.05$ has a very weak magnetic transition at 165 K, that temperature is identified as a TC (Curie Temperature). Finally, for the compounds with $x = 0.07$ and $x = 0.10$ both present a remarkable divergence between ZFC and FC.

In these two compounds is possible to observe the different arrangements that occurs throughout the temperature range. The first ordering corresponds to paramagnetic and is present below 165 K, whereas for the second order is present above 165 K and corresponds to a ferromagnetic order and third order corresponds to an antiferromagnetic order and is at a temperature of 157 K associated to TN (Néel Temperature).

Acknowledgments

1. M. Marezio, *Supercond. Sci. Technol*. **16** (2003) 210-212.

2. Z. Hiroi, J.I. Yamaura, S. Yonezawa and H. Harima, *Phys. C.* **460** (2007) 20-27.

3. M. Deepa, P. Prabhakar Rao, A.N. Radhakrishnan, K.S. Sibi and P. Koshy, *Mater. Res. Bull*. **44** (2009) 1481-1488.

4. K.S. Sibi, A.N. Radhakrishnan, M. Deepa, P. Prabhakar Rao and P. Koshy, *Solid State Ionics.* **180** (2009) 1164-1172.

5. J.A. Díaz-Guillén, A.F. Fuentes, M.R. Díaz-Guillén, J.M. Almanza, J. Santamaría and C. León, *J. Power Sources* **186** (2009) 349-352.

6. G.T. Knoke, A. Niazi, J.M. Hill and D.C. Johnston, *Phys. Rev. B: Condens. Matter Mater. Phys.* **76** (2007) 054439.

7. M. Hirayama, N. Sonoyama, A. Yamada and R. Kanno, *J. Lumin.* **128** (2008) 1819-1825.

8. A. Zhang, M. Lü, Z. Yang, G. Zhou and Y. Zhou, *Solid State Sci.* **10** (2008) 74-81.

9. R.N. Basu, *Recent Trends Fuel Cell Sci. Technol.* (2007) 286-331.

10. R.V. Kumar, H. Iwahara and J.A.L.E.K.A. Gschneidner, in *Handbook on the Physics and Chemistry of Rare Earths*, Elsevier, **28** (2000) 131-185.

11. R.C. Ewing, W.J. Weber and J. Lian, *J. Appl. Phys*. **95** (2004) 5949-5971.

12. M.A. Subramanian, G. Aravamudan and G.V. Subba Rao, *Prog. Solid State Chem*. **15** (1983) 55-143.

13. N. Taira, M. Wakeshima, Y. Hinatsu, A. Tobo and K. Ohoyama, *J. Solid State Chem*. **176** (2003) 165-169.

14. N. Taira, M. Wakeshima, Y. Hinatsu, *J. Solid. State. Chem.* **152** (2000) 441-446.

15. N. Taira, M. Wakeshima, Y. Hinatsu, *J. Phys. Condens Matter* **11** (1999) 6983-6990.

16. M. Ito *et al*., *J. Phys. Soc. Jpn.* **69** (2000) 888-894.

17. M. Ito *et al*., *J. Phys. Chem. Solids.* **62** (2001) 337-341.

18. N. Taira, M.Wakeshima and Y. Hinatsu, *J. Matter. Chem*. **12** (2000) 1475-1479.

19. A. Ehmann, S. Kemmler-Sack, *Mater. Res. Bull.* **20** (1985) 437-442.

20. J.B. Goodenough, A. Hamnet, D. Telles, in: H. Fritzsche, D. Adler (Eds.), *Localization and Metal-Insulator Transitions*, Plenum, (New York. 1985) p.161.

21. T. Yamamoto, R. Kano, Y. Takeda, O. Yamamoto, Y. Kawamoto, M. Takano, *J. Solid State Chem.* **109** (1994) 372-383.

22. M.K. Hass, R.J. Cava, M. Avdeev, J. D. Jorgensen, *Phys. Rev. B.* **66** (2002) 094429-094435.

23. H.M. Rietveld, *J. Appl. Crystallogr* **2** (1969) 65-71.

24. J. Rodríguez-Carvajal, *Physica B: Condens. Matter*. **192** (1993) 55-69.

25. B.J. Kennedy, T. Vogt, *J. Solid State Chem.* **126** (1996) 261-270.

26. R.S. Roth, S.j. Schneider, *J. Res. NBS* **64A** (1990) 309.

27. R.D. Shannon, *Acta Cryst. A* **32** (1976) 751-767.

28. D.R. Beaman, J.A. Isasi, *Electron Beam Microanalysis, Special Technical Publication American Society for Testing and Materials*, **506** (1972) 23.

29. R. Takahashi *et al*., *J. Appl. Phys.* **112** (2012) 073714.

30. S. Yoshii, K. Murata and M. Sato, *J. Phys. and Chem. of Solids.* **62** (2001) 129-134.